

Application of Transformers for Nonlinear Channel Compensation in Optical Systems

Behnam Behinaein Hamgini, Hossein Najafi, Ali Bakhshali, and Zhuhong Zhang

*Ottawa Optical Competency Center, Huawei Technologies Canada, 303 Terry Fox Dr, Kanata K2K 3J1
[behnam.behinaein.hamgini, hossein.najafi, ali.bakhshali, zhuhong.zhang]@huawei.com*

Abstract: In this paper, we introduce a new nonlinear channel equalization method for the coherent long-haul transmission based on Transformers. We show that due to their capability to attend directly to the memory across a sequence of symbols, Transformers can be used effectively with a parallelized structure. We present an implementation of encoder part of Transformer for nonlinear equalization and analyze its performance over a wide range of different hyper-parameters. It is shown that by processing blocks of symbols at each iteration and carefully selecting subsets of the encoder's output to be processed together, an efficient nonlinear compensation can be achieved. We also propose the use of a physic-informed mask inspired by nonlinear perturbation theory for reducing the computational complexity of Transformer nonlinear equalization.

1. Introduction

The impact of nonlinear interference from the fiber Kerr effect and optical/electrical components is a main challenge for high-speed optical systems that limit the achievable transmission rates. This nonlinearity needs to be efficiently handled, specially as the employed constellation sizes are increasing. For the fiber nonlinearity, it is shown that the interference can be equalized in sample or symbol domain by approximating and inverting the nonlinear Schrodinger equation through deterministic models such as digital back-propagation (DBP) [1–3] or perturbation-based nonlinear compensation (PNLC) methods [4, 5].

Alternatively, various solutions are proposed recently in order to exploit deep artificial neural networks (ANN) for nonlinear compensation in optical communications [6–8]. The pattern and medium dependent characteristics of nonlinear propagation make it a suitable case for artificial neural network domain. Specifically, recurrent neural network (RNN) such as long short-term memory (LSTM) are used as more appropriate equalizers of time-series for learning the fiber nonlinearity [9–11] by using received symbol sequences. Attempts are also made to design appropriate ANNs for hardware implementation with real-world applications in mind [12, 13]. However, the sequential nature of RNNs at the core of better performing architectures, is a bottleneck for parallel implantation that is vital for hardware developments of ultra-high-speed optical transmissions.

Recently, Transformers as powerful ANN structures based on self-attention mechanism have been introduced in [14]. Since their birth, these structures are widely employed in various machine learning applications with impressive performance. In fact, Transformers are designed to overcome the limits of sequential nature of RNNs. In particular, unlike RNNs, Transformers are highly parallelizable which makes them greatly suitable for applications in hardware developments for ultra-high-speed optical transmissions.

In this work, we employ Transformers for applications in coherent optical communications. We show that in order to leverage parallel computation and attending directly to the memory across a sequence of received symbols, Transformers with efficient embedding and implementation can be used for nonlinear compensation. We design a Transformer equalizer for nonlinear compensation (Transformer-NLC) with block-processing where one can effectively train and execute the same equalizer over a block of received symbols. This provides the opportunity to share the processing resources while produce a vector of nonlinear distortions which satisfies

the low latency requirements of high-speed coherent optical transceivers. Note that the block-processing with Transformers is in contrast to LSTM models which suffers from the vanishing gradient during train stage as well as increased latency in the inference stage over long blocks of symbols [12].

Furthermore, the use of a physic-informed mask according to the nonlinear perturbation theory is presented in order to make the attention matrix sparse. By employing two-dimensional relations modeled as a mask matrix which highlights the importance of the combinations of symbols for nonlinear estimation, savings in computational complexity are achieved specially at regions with very limited resources.

The remainder of this paper is organized as follows: In Section 2, the base of nonlinear compensation for fiber channel along with the basic structure of Transformers are briefly discussed. In Section 3, the building blocks of the NLC with Transformers for single symbol and a block of symbols are introduced. Also, the impact of perturbation mask for reducing the computational complexity of Transformers is explained. Next, numerical results are presented in Section 4 and finally, we summarize the paper in Section 5.

2. Preliminaries

2.1. Nonlinear Compensation in Coherent Optical Systems

Considering the dual-polarization evolution of optical field over a fiber link according to the Manakov equation [15], the nonlinear propagation impact can be shown as the right-hand side of the following equation:

$$\frac{\partial u_{x/y}}{\partial z} + \frac{\alpha}{2} u_{x/y} + j \frac{\beta}{2} \frac{\partial^2 u_{x/y}}{\partial t^2} = j \frac{8}{9} \gamma \left[|u_x|^2 + |u_y|^2 \right] u_{x/y}, \quad (1)$$

where $u_{x/y} = u_{x/y}(t, z)$ represents the optical field of polarization x and y , respectively, α is the attenuation coefficient, β is the group velocity dispersion (GVD), and γ is the nonlinear coefficient. This Kerr nonlinear impact can traditionally be equalized through deterministic nonlinear models by approximating and inverting the equation through DBP [1–3] where the fiber is modeled as a series of linear and nonlinear sections through first-order approximation of Manakov equation. Also, by employing the perturbation analysis [4], the optical field can be represented as the solution of a linear term plus a nonlinear perturbation term in symbol domain and in a lumped stage. In fact, the first-order perturbation term can be modeled as the weighted sum of triplets of symbols plus a constant phase rotation [5, 16].

Various solutions has been introduced to employ machine learning for the fiber nonlinearity compensation(e.g. [6–11]) in which one can learn the equalization process through data. These artificial neural network nonlinear compensation (ANN-NLC) solutions include learned-DBP, using triplets of symbols for PNLC with basic neural networks, and using soft-symbols in deep neural networks. Furthermore, data-driven ANN solution provides a more general and flexible approach while giving us the potentials for large simplifications in computational complexity with efficient quantization of the network [17].

A basic block diagram for a receiver side equalization process is presented in Fig. 1 where after the conventional linear processing for the coherent optical receiver, the preprocessing buffer generates appropriate inputs for an ANN method. This can be seen in form of calculated PNLC triplets for a perturbation-based method, or a vector of soft symbols at the end of Rx-DSP chain for a deep artificial neural network nonlinear compensation. Assuming the first-order perturbation is the dominant term, an scaler can also be used. Hence, nonlinear compensation estimated values can be scaled in case the training and inference are done at different launch powers. Moreover, transfer learning can be performed by updating only a part of the ANN for the changes in the transmission scenarios [18].

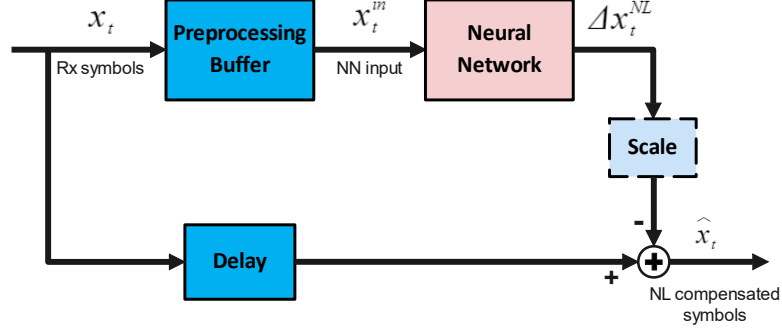


Fig. 1. Receiver symbol-domain diagram for neural network nonlinear compensation.

2.2. Transformers

Transformers were introduced in [14] based on the self-attention mechanism and have been employed in different fields of machine learning including language modeling, vision, audio, and time series processing with impressive performance while being appropriate for parallel implementation. Specifically, a Transformer processes all symbols in parallel and provides direct interactions among symbols in an input sequence which makes it capable of capturing memories more efficiently compared to an LSTM where the memory is handled sequentially. This makes Transformers highly matched for applications in hardware developments of ultra-high-speed optical transmissions.

A vanilla Transformer consists of an encoder and decoder architecture for language processing. However, for our application of fiber nonlinear equalization, we just employ the encoder part of a Transformer which is depicted in Fig. 2. This architecture consists of a module that generates the embeddings, a positional encoder, L stacked layers of multi-head attention (MHA) and position-wise feed-forward network (FFN), and an output module at end that can be an MLP to generate the estimated nonlinear interference associated to real and imaginary parts of the equalized output symbol sequence. There are also a residual connection and layer normalization at each layer.

The attention function is at the core of a Transformer where a query-key-value vector model is employed. In fact, the mapping across those three vectors can be calculated by their interactions according to various methods including, additive attention [19], dot-product attention [14], kernel-based attention [20], or through a set of learned position biases [21]. Specifically for the scaled dot-product self-attention, given queries $Q \in R^{N \times d_K}$, keys $K \in R^{M \times d_K}$, and values $V \in R^{M \times d_V}$, one can write:

$$A = \text{softmax}\left(\frac{QK^T}{\sqrt{d_K}}\right) \quad (2)$$

$$\text{Attention}(Q, K, V) = AV$$

where N and M are the length of queries and keys (values), respectively, d_K is the dimension of keys and queries, d_V is the dimension of values, and A is the *attention matrix*. It should be noted that the softmax is preformed row-wise in Eq. (2). The term $\sqrt{d_K}$ is also added to mitigate the gradient vanishing problem of the softmax function. Note that in the encoder architecture as employed in our work, queries, keys, and values are obtained from the same vector from the input sequence. Moreover, a sequence of learned embeddings can be used instead of initial input sequence as the input for the first layer of the encoder since the embedding generating module generally produces better input features.

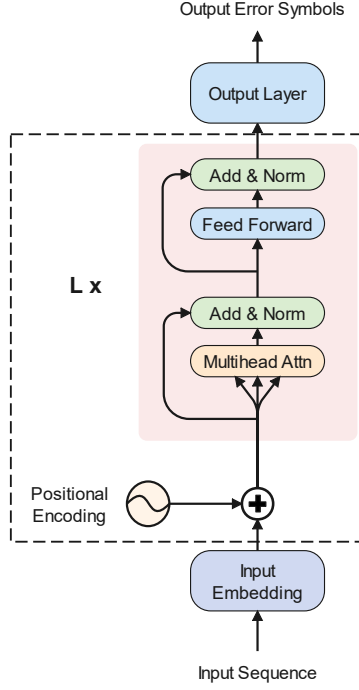


Fig. 2. Transformer encoder architecture.

Transformer architecture utilizes a multi-head attention mechanism to map the original queries, keys, and values (d_{model}) into lower-dimension spaces, d_K, d_V using linear layers where $d_K = d_V = d_{model}/h$, and h is the number of heads. After applying the self-attention showed in Eq. (2), the output of multi-head attentions are concatenated, passed through a linear layer, and fed into the position-wise FFN module. The FFN is a fully connected feed-forward module located at every layer of the encoder where it is applied to each position, similarly. This module consists of two linear layers and a ReLU activation as

$$\text{FNN}(x) = \text{ReLU}(xW_1 + b_1)W_2 + b_2 \quad (3)$$

where $W_1 \in \mathbb{R}^{d_{model} \times d_{ff}}$, $W_2 \in \mathbb{R}^{d_{ff} \times d_{model}}$, $b_1 \in \mathbb{R}^{d_{ff}}$, and $b_2 \in \mathbb{R}^{d_{model}}$.

Transformers also use residual connection and a layer normalization after each pair of attention and FNN modules as:

$$\begin{aligned} Y &= \text{LayerNorm}(\text{MHA}(X) + X) \\ Z &= \text{LayerNorm}(\text{FFN}(Y) + Y), \end{aligned} \quad (4)$$

where the layer normalization is performed after the residual addition. Note that changing the layer normalization position in the network leads to different Transformer structures. This may impact training behavior of the Transformer in general and requires learning rate optimization [22]. However, in this work we use the original post layer normalization structure which needs a warm-up stage for the learning rate. Furthermore, For positional encoder, we use a positional encoder as introduced in [14].

3. Transformers for Nonlinear Compensation

3.1. Model Architecture

In this work, we use the above Transformer encoder architecture to estimate the nonlinear distortions in the received symbols. The overall design for the nonlinear channel equalization is depicted in Fig. 3. Due to the channel memory and pattern-dependency over the transmitted sequence, for predicting the nonlinear distortion for a target symbol, it is required to process several symbols before and after it. We show the number of these extra symbols from each side of the target symbol by tap-size value t . For the single symbol processing, the model's input has a dimension of $R^{(2t+1) \times 4}$ where t is the tap size and 4 is the number of input components from the optical domain, X_I, X_Q, Y_I, Y_Q . At first, an embedding generator module maps the sequence of received symbols into $R^{N \times d_{model}}$, where depending on the type of embedding generator module, N can be equal or different from $2t + 1$, and d_{model} is the embeddings dimension. The case where N is different from $2t + 1$ will be discussed later when we discuss a CNN embedding generator. Next, a Transformer is used as the core for the nonlinear equalization. The dashed block in Fig. 2 corresponds to the Transformer block that operates on the generated embeddings.

The next module processes the Transformer's output to generate the equalizer's nonlinear distortion estimations. By using a Transformer, we can process N input embeddings simultaneously and produce N output representations. However, since we are interested in computing the distortion for a target symbol s , we may not need all the N output representations and a subset of them may suffice. In other words, in order to output the nonlinear distortion for symbol s , we may only use the Transformer's output representation for s or use a window of representations around s . We call these extra representations the *neighbors* of s . The impact of optimizing this neighboring window of size W on the design is explained more in Section 3.4. Specifically, the selected window of representations are fed into an MLP module consists of a linear layer ($\in R^{W \cdot d_{model} \times 2}$), a leaky ReLU nonlinear activation function with negative slope of 0.2, a second linear layer ($\in R^{2 \times 10}$), a leaky ReLU nonlinear activation function with negative slope of 0.2, and a third linear layer ($\in R^{10 \times 2}$). The last layer has two outputs that generates E_{X_I} and E_{X_Q} , the estimated nonlinear distortions corresponding to the target symbol.

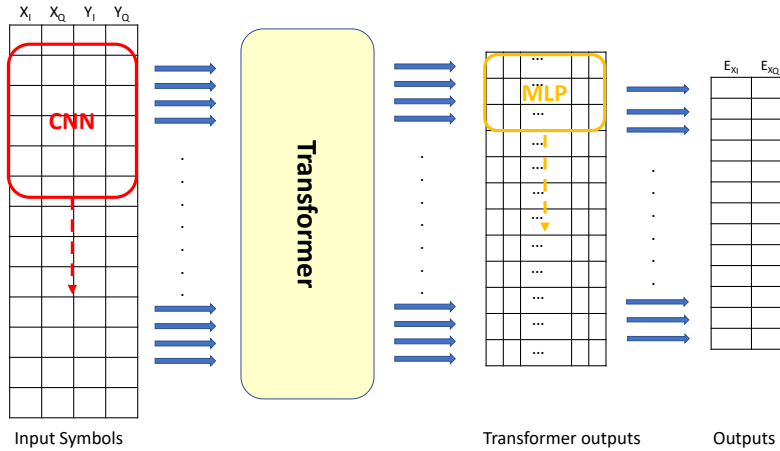


Fig. 3. The overall model architecture for the nonlinear channel equalization. From left to right: the CNN generates input embeddings which are processed by the Transformer to generate output representations. These outputs are then fed into an MLP to generate the estimated nonlinear distortions E_{X_I} and E_{X_Q} .

Considering the ultra high-speed optical applications, parallel and vector processing (instead of sequentially processing of a single symbol) is vital to achieve high throughput out of digital processing stage. Therefore, it is required to employ the NLC equalizer over blocks of data in the inference stage. This requirement is challenging for RNNs and LSTM equalizer models, since training in sequential manner over a long block length would result in a vanishing gradient problem as well as increasing delays in the inference stage. One solution that has been used recently is to train the network with one symbol processing structure, then by using approximations on hidden states, produce a vector of outputs in the inference stage. However, the approximate model still suffers from a long delay which will limits the real-world applications of ANN-NLC. On the other hand, Transformers in contrast to LSTMs, have the benefit of being trainable on very long sequences of symbols without the vanishing gradient issue or delay of sequential processing, which yields the advantage of accelerating the training process by a large factor. Here, we complete the Transformer-NLC design by employing a sequence of symbols to produce a series of associated nonlinear distortions at the output, concurrently. Specifically, using Transformers with block-processing one can efficiently train and operate the same accurate equalizer over a block of received symbol to share the processing resources while producing a block of outputs that can satisfy low latency requirements of coherent optical transceivers.

For processing a block of symbols for equalization, the training/inference samples are created by selecting a block of b symbols. In order to maintain the quality of equalization at the beginning and end of the block, we append extra symbols at the head and tail of the block; effectively expanding the selected symbols with extra $2t$ symbols at each side. Hence, each input sequence length is equal to $b + 2t$. This sequence of symbols passes through the embedding generator module which produces $b + \ell$ embeddings (the exact value of ℓ will be explained later). These embeddings are then fed into the Transformer where $N = b + \ell$ outputs are generated. The output module (MLP in the Fig. 3) generates b estimated nonlinear distortions which are used for computing the loss in the training stage. This loss is generated as the mean squared differences between b estimated nonlinear distortions and b target ones. Through back-propagation, the optimizer uses this loss to modify the weights in the training stage. With this approach, training can be accelerated by a large factor since instead of training over one symbol at a time, the model is trained on b symbols at each training iteration. In addition, in the inference (equalization) stage, the Transformer generates b nonlinear distortions at once through operations that are highly parallelizable. Therefore, we are able to utilize the Transformer structure better than LSTM models in the training stage as well as reduce the computational complexity per symbol by employing block-processing. This can be seen from the following equation where the computational complexity of the attention matrix is expressed as a function of block size b :

$$RMPS_{att-blk} = \frac{h(b + \ell)^2 d_k + 3h(b + \ell)^2}{b}. \quad (5)$$

where h is the number of heads and RMPS stands real multiplications per symbol. In analyzing the computational complexity, we only consider the multiplication operations and do not include the additions. Hence, RMPS is used as the complexity metric in this work. The first term in the above equation is the complexity of computing QK^T , and the second term is the complexity of division by $\sqrt{d_k}$ and softmax computation. In a vanilla Transformer, the size of d_K and d_V are chosen as d_{model}/h . In our studies, we also explore the configurations where d_K and d_V are equal to d/h where d may not be equal to d_{model} . This case is particularly of interest since for $d < d_{model}$, we can reduce the computational complexity. Note that, we exclude the ReLU and leaky ReLU's computational complexities in our analysis, since their hardware implementations are fairly simple and requires very little resources. Note that the reduction factor of b also exists in the other layers including FFN and output layer. Assuming ℓ and h constants, for large b , the overall complexity in Eq. (5) is approximately $O(bd_k)$ per symbol which is in fact linear in block size b .

3.2. Embedding

Our studies have shown that the Transformer faces serious challenges in learning the relationships between symbols when they are directly fed into. Hence, we need to create good representations, commonly known as *embeddings*, of the input components, X_I, X_Q, Y_I, Y_Q , prior to feeding them to the Transformer. We have explored two main classes of ANN models for generating the embeddings, an MLP and a CNN. For the MLP architecture, we examine two configurations. In the first one, an MLP with only one linear layer is used. In the second configuration we employ a multi-layer MLP comprising a linear layer, a Leaky ReLU nonlinear activation with the negative slope of 0.2, and another linear layer. Note that over the input sequence, the MLPs are applied to each position, similarly. Using these MLPs we project the input symbols ($R^{(2t+b) \times 4}$) into embeddings with dimension $R^{(\ell+b) \times d_{model}}$ where $\ell = 2t$, and t is the tap size as defined by the number of symbols on each side of the target symbol(s).

We also explore the use of CNNs for creating embeddings since they have shown great potential for generating features from sequences. We use a CNN with one layer of one-dimensional convolutional layer with a kernel size of k , four input channels, d_{model} output channels, and a stride of one, followed by a leaky ReLU nonlinear activation function with negative slope of 0.2. The CNN generates embeddings of dimension $R^{(\ell+b) \times d_{model}}$ where $\ell = 2t - k + 1$.

Note that we use ℓ to unify our math notation for representing computation complexities for Transformers with either MLP or CNN embeddings-generator modules, and one should note that ℓ is equal to $2t$ for MLP generated embeddings and $2t - k + 1$ for CNN generated embeddings with the kernel size of k .

3.3. Mask

The attention matrix can be *masked* for variety of reasons, for example to introduce some properties into the model such as preserving the auto-regressive property by employing a proper mask. Masking can also be used to reduce the complexity of attention calculations (A in Eq. (2)). One approach is to make the attention matrix, A , sparse so the zero elements need not to be computed or stored [23, 24]. Note that computing the attention is a complexity bottleneck in the vanilla Transformer for long sequences.

In this work, we propose a method to make the matrix A sparse according to a physic-informed mask from the perturbation theory. As briefly discussed in Section 2, the optical field can be represented as the solution of a linear term plus a nonlinear perturbation term in symbol domain. The perturbed term can be represented as the weighted sum of symbol triplets assuming pulse spreading (memory) that is much greater than the symbol duration due to the accumulated dispersion impact [5]. Hence, the perturbation term for the target symbol at the middle of sequence can be simplified as:

$$\Delta u_{x/y} = \sum_{m,n} P_0^{3/2} (A_{n,x/y} A_{m+n,x/y}^* A_{m,x/y} + A_{n,y/x} A_{m+n,y/x}^* A_{m,x/y}) C_{m,n} \quad (6)$$

where P_0 is the optical launch power, $A_{.,x/y}$ is the sequence of complex transmitted symbols, and $C_{m,n}$ is the nonlinear perturbation coefficient.

Specifically, the perturbation coefficients $C_{m,n}$ show which combinations of symbols are more important to estimate the nonlinear interference. Therefore, we can use this two-dimensional relations inside our attention matrix as a mask to reduce the computational complexity. Considering the hyperbolic form of the perturbation coefficients, we can use a two-dimensional link-independent criteria as a mask by selecting a subset of elements in attention matrix. As an example, we use the following relation as in [6] in the numerical result:

$$|n| \leq \min \left(\frac{\rho \lceil \ell/2 \rceil}{|m|}, \left\lceil \frac{\ell}{2} \right\rceil \right) \quad (7)$$

where $\lceil \cdot \rceil$ represents the ceiling function, ℓ is the maximum of m and n , and ρ restrains the maximum of (m, n) pairs. Since the Transformer also needs to determine the interaction between symbols, based on the above equation, we propose only using the elements of attention matrix $A_{m,n}$ that satisfy the m and n relation in Eq. (7), where m and n are row and column indices, respectively, and make all the other elements zeros. To implement this approach in the single symbol processing, in the simulation, we add a mask matrix, M^{indv} to $QK^T/\sqrt{d_k}$. The matrix, M^{indv} , has the same size as QK^T and is generated such that the elements that satisfy the relationship between m and n as in Eq. (7) are filled by zeros and those that do not are filled with the negative infinity. This guaranties that the elements in attention matrix that do not meet Eq. (7) are set to zeros since the softmax operator maps the negative infinity to zero. The elements that their indices meet Eq. (7) are not affected by the mask since adding a zero to an element has no effects on the softmax's output.

The algorithm for generating M^{indv} is shown in Alg. (1) for the single symbol processing. Depending on the values of tap size t and mask hyperbolic parameter ρ , the number of non-zero elements in the mask varies and consequently the number of operations needed for computing the attention matrix changes. Figure 4 shows the attention mask for the single symbol processing for different values of t and ρ .

Algorithm 1 Algorithm for generating mask for the single symbol processing

Input: ℓ, ρ

Output: M^{indv}

M^{indv} = matrix of size $(\ell + 1) \times (\ell + 1)$

$M_{i,j}^{indv} = -\infty, i, j \in 1 \cdots \ell + 1$

for $m = -\ell/2$ to $\ell/2$ **do**

for $n = -\ell/2$ to $\ell/2$ **do**

if $m \neq 0$ **and** $|n| \leq \min\left(\frac{\rho \lceil \ell/2 \rceil}{|m|}, \lceil \frac{\ell}{2} \rceil\right)$ **then**

$M_{\ell/2+m+1, \ell/2+n+1}^{indv} = 0$

end if

end for

end for

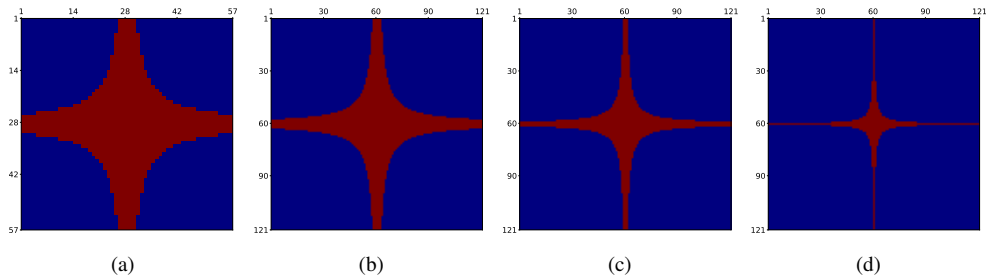


Fig. 4. Attention masks for the cases where the output error only computed for the central symbol. The red area shows the values that are zeros (unmasked) and the blue area shows the values which are negative infinity (masked). (a) $t = 32$ and $\rho = 2.6$, (b) $t = 64$ and $\rho = 2.6$, (c) $t = 64$ and $\rho = 1.3$, and (d) $t = 64$ and $\rho = 0.4$. The ratio of the number of unmasked (zero) elements to the total number of elements is 0.31, 0.19, 0.10 and 0.04 for figure (a), (b), (c), and (d), respectively.

In summary, with the assumption that computation of the attention matrix can be implemented such that the computations are only carried out for the non-zero values in the attention matrix

(corresponding to zero values in the proposed mask), we can reduce the computational/space complexity of attention to $O(\hat{N}d_k)$ where \hat{N} is the number of non-zero elements in the attention matrix.

Next, we extend the mask approach introduced above to the block-processing case. The method we propose here is based on computing a union-like combination of individual symbol's mask. The algorithm for computing the mask for the block-processing approach is shown in Alg. (2). Note that the size of the block mask matrix, M^{block} , is $(\ell + b) \times (\ell + b)$ and the size for individual symbol's mask, M^{indv} , is $(\ell + 1) \times (\ell + 1)$, where individual mask is computed using Alg. (1). Two block masks are depicted in Fig. 5 where the block mask for a model with $t = 64, b = 128, \rho = 2.6$ is shown in Fig. 5a and Fig. 5b shows a block mask for a model with $t = 64, b = 128, \rho = 0.4$. As can be seen from the figure, the choice of ρ does not have a huge impact on the shape of mask, which in fact is not surprising since the block mask is generated by stacking individual masks on each others. The ratios of the unmasked (zero) elements to the total elements are 0.34 and 0.31 for $\rho = 2.6$ and $\rho = 0.4$, respectively.

For large block sizes, the ratio of the number of unmasked (zero) elements to the total number of elements decreases. Fig. 5c shows the impact of increasing the block size to 4096. In this case, the ratio of the number of unmasked (zero) elements to the total number of elements is less than 0.03. Therefore, if one can implement matrix multiplications in such a way that attention terms corresponding to the negative infinity elements in the mask are avoided, then the complexity of computing the attention matrix can be reduced by 97 percent. Finally, Fig. 5d shows the plot for ratio of the number of unmasked (zero) elements to the total number of elements versus block size. As it can be seen from this figure, the ratio first increases and then decreases as the block size increases. It should be noted that the choice of the block size needs to be optimized according to the system requirements in terms of throughput and latency, and hence, it cannot be increased too much due to increasing required memory and computational complexity of Transformers. A detailed discussion on the impact of block size is given in Appendix A.2.

Note that to give some numerical examples of the effect of mask on softmax input, several two-dimensional heat maps of $(QK^T)/\sqrt{d_k}$ for Transformer with and without masks are shown in Appendix B.

3.4. Using Neighbors at the Output Layer of Transformer

For computing nonlinear distortion from the output of the last layer of Transformer, we employ an MLP as explained in Section 3.1. To compute each nonlinear distortion s_i , one option is to give the corresponding Transformer-generated representation, r_i , to the MLP. However, due to the dependency of symbols on each others, we observe that if for each symbol s_i , we also provide few representations around r_i to the MLP, it can compute s_i more accurately. We call this approach *window processing* and while it increases the model's performance, it does not increase the computational complexity hugely if the window size is not very large (which does not need to be as shown in our simulation results). To see the impact of window processing on the computational complexity, first consider the model without window processing. With the dimension of representation for each r_i as d_{model} , the first layer of the MLP has d_{model} inputs and the computational complexity of the MLP is of order of $O(d_{model})$ per symbol. Now in window processing, for each symbol s_i , in addition to the r_i , w positions on each side of r_i is also fed into the output MLP which will increase the complexity by order of $2w$. However, since w is fixed in our Transformer design, the computational complexity is still of order of $O(d_{model})$ per symbol. Finally, note that the use of neighboring representations at the output of the Transformer can also be exploited by other methods such as using a one-dimensional CNN as the first layer of the output module.

Algorithm 2 Algorithm for generating mask for blocks.

Input: ℓ, ρ, b

Output: M^{block}

M^{block} = matrix of size $(\ell + b) \times (\ell + b)$

$M_{i,j}^{block} = -\infty, i, j \in 1 \dots \ell + b$

M^{indv} = generate mask for one symbol using Alg. 1

for $i = 1$ to b **do**

$M_{i:i+\ell, i:i+\ell}^{block} = \max_{\text{element-wise}} (M_{i:i+\ell, i:i+\ell}^{block}, M^{indv})$

end for

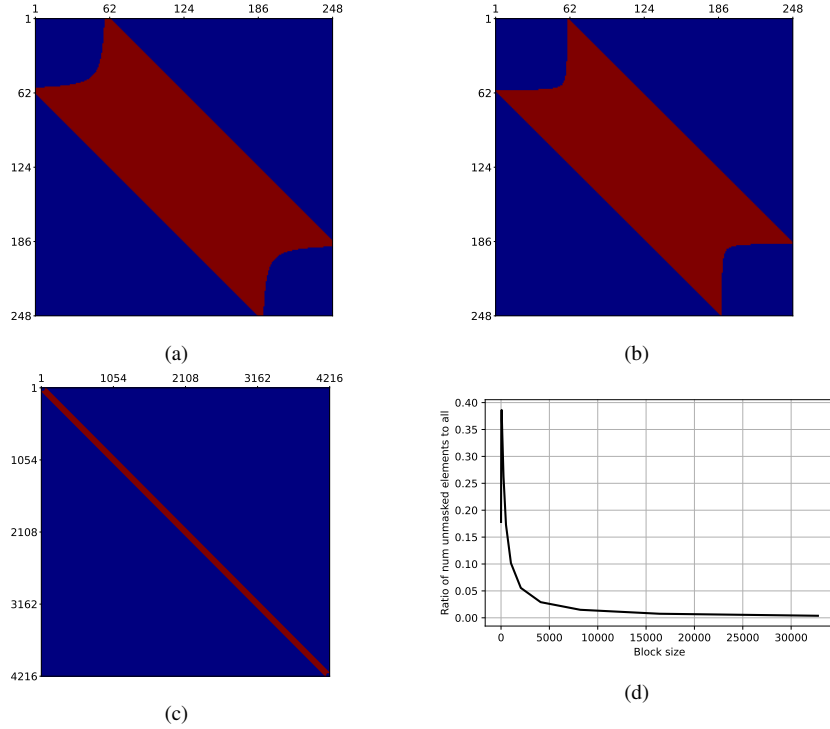


Fig. 5. Masks for blocks. (a) shows a block mask with $t = 64, b = 128, \rho = 2.6$ while (b) depicts a block mask with $t = 64, b = 128, \rho = 0.4$. (c) and (d) show the impact of increasing the block size on the ratio of the number of unmasked (zero) elements to the total number of elements. (c) shows the mask where the block size is 4096, $t = 64$, and $\rho = 2.6$. The blue area shows the elements with negative infinity values and the red shows zero elements. (d) shows the ratio of the number of unmasked (zero) elements to the total number of elements versus block size.

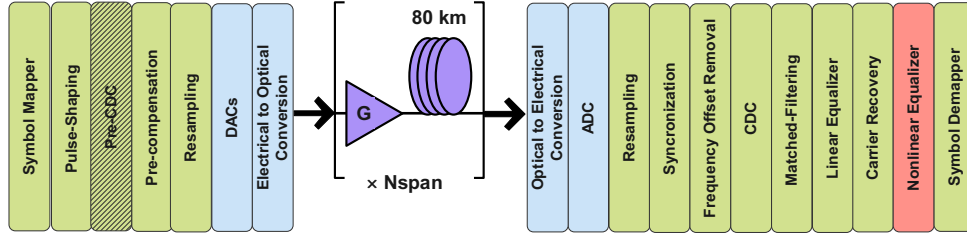


Fig. 6. System model with nonlinear equalizer at receiver side.

4. Numerical Results

4.1. System Model

The system model for generating the simulation results includes typical Tx, channel, and Rx modules for a single-carrier transmission scenario. Specifically, we consider digital chromatic dispersion compensation modules both at Tx and Rx side. To focus on fiber nonlinearity, we consider ideal electrical components and Mach-Zhender modulator. Also, DACs/ADCs are ideal with no quantization or clipping effects. The dual polarization fiber channel is modeled by split-step Fourier method [25] with adaptive step-size and maximum nonlinear phase-rotation of 0.05 degree to ensure sufficient accuracy. At the Rx side, the sequence output from carrier recovery (CR) are used to train and evaluate Transformer-based nonlinear equalizer. Standard DSP algorithms are employed for detection and processing of the received signal at the Rx. The block diagram for such system is depicted in Fig. 6. Note that, to keep the ability of conventional coherent receiver for phase correction under correlated phase-noise (which is coming from nonlinear propagation in our case), we deployed the carrier recovery before ANN-NLC module. This ensures that the linear equalization provides nonlinear phase compensation capability of a coherent receiver without a dedicated NLC equalizer. Hence, the neural network compensation gain is given on top of the best linear performance.

To evaluate and optimize different algorithms, we focus on two cases with single-channel system. The first one is operating at 32Gbaud 16QAM modulation where the link consists of 40 spans of standard single-mode fiber (SSMF) of 80km length. The second case uses 42Gbaud 64QAM modulation format with 12 spans of SSMF each 80km. Each span is followed by an optical amplifier with 6 dB noise figure. The signals are pulse shaped by a root-raised cosine function with a roll-off factor of 1/16. Furthermore, we consider a symmetric dispersion map, in which half of total dispersion is digitally pre-compensated at the transmitter side. The training and evaluation stage is performed at 2 dBm and 3 dBm launch powers for the two cases, respectively. This is close to the optimal launch power for each case when DBP at 2 sampler-per-symbol and 1 to 3 steps-per-span are employed to benchmark these results.

4.2. Numerical Setup

We perform a wide grid search over hyper-parameters of the Transformer consisting of hundreds of models for each of the two setup cases. Standard Rx-DSP output for 2^{19} and 2^{18} symbols were used in the training and evaluation of these models, respectively. A permuted congruential generator (PCG64) with different seeds for training and evaluation stages was employed. Models are trained for a mini-batch size of 512 using Adam optimizer with a learning rate scheduler that includes a warm-up, and a mean-squared-error loss function. Early stopping is used to stop the training if the model performance has not improved over 100 epochs. Note that the proposed ANN-NLC equalizers estimate the nonlinear distortions in one polarization. However, due to

the symmetric nature of signal propagation in fiber medium, it has been shown that the same model can be used to generate the nonlinear error estimates for the other polarization by simply swapping input signals. This enables efficient learning of a generalized model that performs on both polarizations.

Parameters and components in a Transformer architecture can be varied in order to explore performance and computational complexity of different realizations. Among these parameters, we ran a grid search on the following hyper-parameters: tap size, d_{model} which we will call *hidden size*, key size, number of heads, number of encoder layers, number of outputs for the first layer of point-wise FFN which is called *FFN's hidden size*, presence or absence of mask, and output layer window size. We implemented the search in two steps: First, for each hyper-parameter we ran a specific grid search where we selected a wide range for that specific hyper-parameter while only few values for the remaining parameters were included. In the second step, we chose some of the best values from the first run and performed a grid search on the combination of those values. As discussed earlier, the type of network that generates the embeddings is important. Hence, we carried out a separate grid-search on the impact of block size and embedding generator networks on a smaller grid which is presented in the Appendix A (Sections A.1 and A.2). Table 1 shows the summary for the selected values of the grid search in the second step. We employed separate search spaces for 16QAM and 64QAM cases tailored to their propagation mediums.

Table 1. Transformer's hyper-parameters and their values used for the grid search.

Hyper-parameter	Grid Search Values for 16QAM	Grid Search Values for 64QAM
tap size	$\in [8:96]$	$\in [16:64]$
hidden size	$\in [8:96]$	$\in [16:96]$
key size	$\in [8:64]$	$\in [16:64]$
number of heads	1, 2, 4	1, 4
number of encoder layer	1, 2, 3	1, 2, 3
FFN's hidden size	32, 64	64
window size	1, 7, 15	1, 7, 11
mask	None, $\rho = 2.6$	None, $\rho = 2.6$

4.3. Analysis of the Performance versus Complexity Trade-off for 16QAM Setup

The numerical results for hyper-parameters grid search in the 16QAM case is given in Fig. 7. This figure shows the scatter plot for the performance, represented by the quality metric Q, versus complexity, represented by RMPS, for all model variations obtained from sweeping over hyper-parameters in Table 1. We use blue and red colored dots to show the results for the Transformers with and without mask, respectively. Additionally, the blue and red lines in the figure illustrate the envelopes associated to the best performing Transformers with and without mask, respectively. All Transformers are designed for a block size of 128 symbols. As seen from the figure, Transformers can achieve very good nonlinear compensation performance as the best models in 16QAM setup have improved Q from 6.7 dB (Linear case) to more than 8.8 dB, a 2.1 dB improvement at the training launch power of 2dBm. In addition, even at the lower complexities where the performance has been decreased, we still retain a good nonlinear compensation capability. Moreover, using a mask does not have a significant degrading impact on the performance in general while it can particularly boost performance at the lower complexity regions compared to the Transformers without mask.

To further study the nonlinear compensation performance of these models, several of them are selected as examples from different regions close to the envelope of performance versus complexity trade-off graph. Table 2 shows the hyper-parameters for the selected model in each region for the 16QAM setup. To better illustrate these results and have a clearer picture of the effects of proposed masks on the performance and complexity of the models, results from the cases with mask and without masks are also presented here.

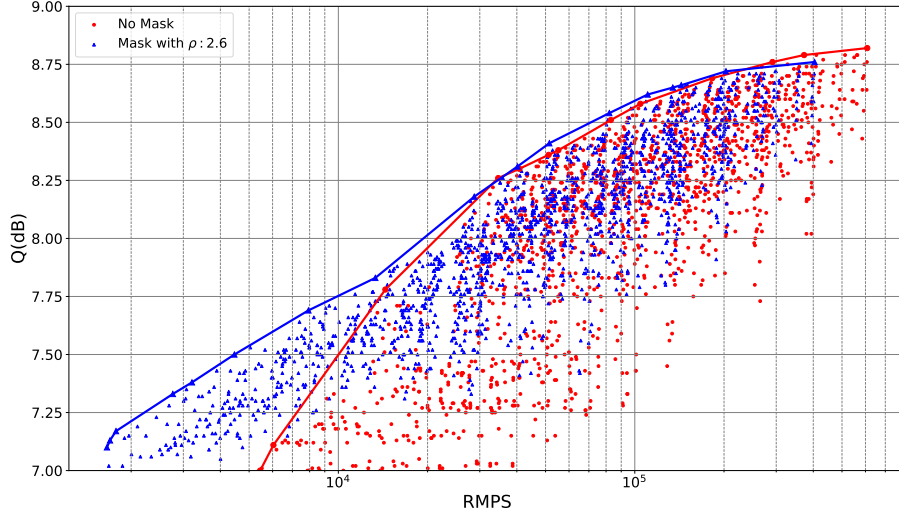


Fig. 7. Performance vs. complexity tradeoff for the 16QAM setup for the grid search shown in Table 1. The models were trained and evaluated at 2dBm launch power. The red dots show the results for the models that did not use the proposed mask while blue triangles represent the ones with the proposed mask.

Table 2. Hyper-parameters for the selected models at three different performance vs. complexity regions for 16QAM setup.

Hyper-parameter	Region 1	Region 2	Region 3
tap size	96	64	16
hidden size	96	64	16
key size	64	32	16
number of heads	4	4	4
number of encoder layer	3	2	2
FFN's hidden size	64	32	32
window size	15	7	7

Fig. 8 shows the performance vs launch power for the three selected models at different computational complexity regions. We also provide DBP's performance results at two sample-per-symbol with different steps-per-span(StpS) to benchmark the proposed Transformer structures. Note that, the complexity comparison with other NLC methods such as DBP is not performed here since an accurate comparison requires the development of efficient hardware-friendly versions of these designs after model compression, pruning, and weight quantization. Also, as noted before, the DBP's performance here provides an upper-bound since it is performed at 2 samples per symbol with no other component or channel impairments involved where it can efficiently reverse the simulated nonlinear channel.

We observe that the selected models demonstrate good generalization and can provide nonlinear performance gain over a wide range of launch powers. Additionally, compared to linear compensation, the best performing model improves the optimal launch power by 1.5 dB while the maximum Q-value at the optimal launch power is also boosted by 1.5 dB (from 7.3 dB at 0.5 dBm to 8.8 dB at 2 dBm). Table 3 illustrates the summary of the results for the above-selected regions at 2 dBm launch power as an example. The reduction in complexity with improved performance is notable with use of mask for Region 3 at the lowest complexity region.

Table 3. Summary of results evaluated at 2dBm launch power for the selected 16QAM models.

	Q	No Mask		Mask with $\rho = 2.6$	
		Q_{NN}	RMPS (K)	Q_{NN}	RMPS (K)
Region 1	6.67	8.82	608	8.76	404
Region 2	6.67	8.54	129	8.51	81
Region 3	6.67	7.31	22	7.68	9

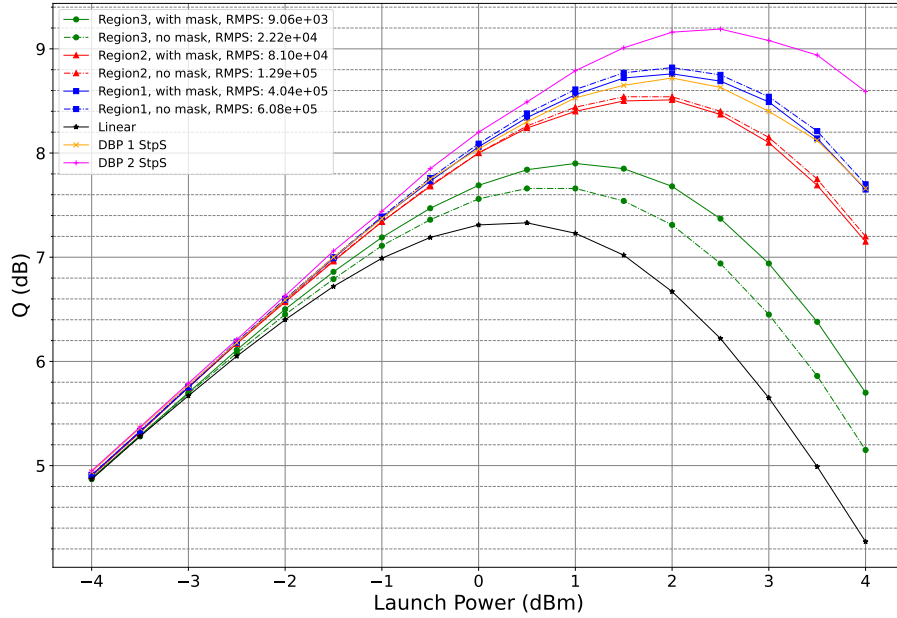


Fig. 8. Performance of the three selected 16QAM models of Table 2 at various launch powers. The results of the linear compensation and DBP with 1 and 2 steps per span are also shown in the figure.

4.4. Analysis of the Performance versus Complexity Trade-off for 64QAM Setup

As for the previous case, we also performed a grid search for 64QAM setup. Fig. 9 shows the scatter plot for the performance versus complexity, for all model variations by sweeping over the hyper-parameters for 64QAM in Table 1. In the figure, blue and red colored dots are used to show the results for Transformers with and without mask, respectively, and blue and red lines are employed to depict the envelopes associated to the best performing Transformers with and without mask, respectively. All models for the 64QAM setup were trained with a block size of 128 symbols. From Fig. 9 we can see that the Transformers provide an excellent nonlinear compensation performance as the best models have improved Q from 6.5 dB (Linear case) to 8.17 dB, a 1.67 dB improvement at the training launch power of 3 dBm. Also in this setup, using a mask boosted the performance at the lower complexity regions with almost no performance loss in general.

We select three models as examples from different regions close to the envelope of the performance versus complexity trade-off graph to further investigate the nonlinear compensation performance of these models. Table 4 shows the hyper-parameters for the selected model in

each region. Fig. 10 shows the power-sweep performance for the three selected models as well as DBP's results at two sample-per-symbol with different steps-per-span(StpS) to benchmark the proposed Transformer structures. This figure shows that the selected models achieve good generalization and provide great nonlinear performance gains over a wide range of launch powers. As it can be seen, compared to the linear compensation, the best performing model improves the optimal launch power by 1.5 dB while the maximum Q-value at the optimal launch power is also increased by 1.26 dB (from 6.91 dB at 1.5 dBm to 8.17 dB at 3 dBm). Finally, Table 5 shows the summary of results for the above-selected regions at 3 dBm launch power as an example. As it can be seen, in Region 1, the model with the mask performs as well as the model without a mask while has a lower RMPS. In Region 3, the use of mask resulted in reduction in the complexity while improved the performance at the lowest complexity region.

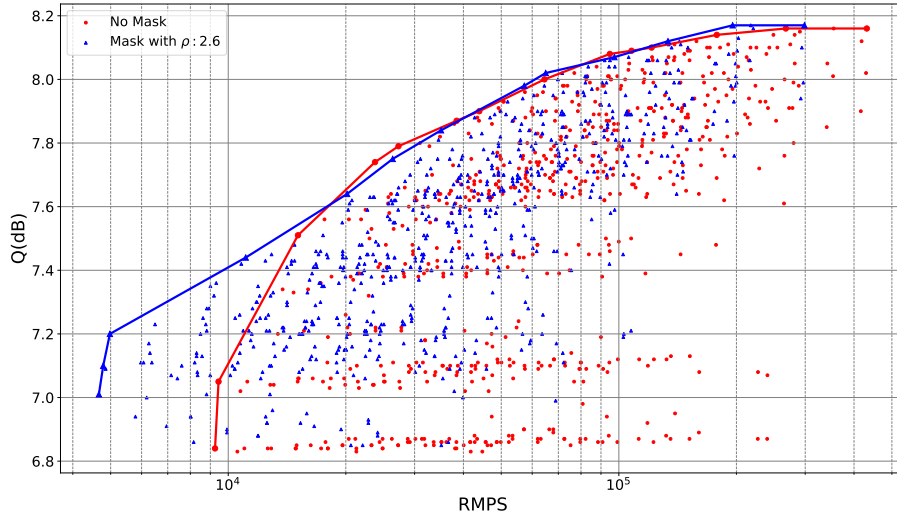


Fig. 9. Performance vs. complexity trade-off graph of the 64QAM setup for the grid search shown in Table 1 . The models were trained and evaluated at 3dBm launch power. The red dots show the results for the models that did not use the proposed mask while blue triangles represent the ones with the proposed mask.

Table 4. Hyper-parameters for the selected models at three different performance vs. complexity regions for 64QAM setup.

Hyper-parameter	Region 1	Region 2	Region 3
tap size	64	32	8
hidden size	96	64	16
key size	32	32	16
number of heads	4	4	4
number of encoder layer	3	1	1
FFN's hidden size	64	64	64
window size	11	11	7

Table 5. Summary of results evaluated at 3dBm launch power for the selected 64QAM models.

	Q	No Mask		Mask with $\rho = 2.6$	
		Q_{NN}	RMPS (K)	Q_{NN}	RMPS (K)
Region 1	6.50	8.16	268	8.17	196
Region 2	6.50	7.9	50	7.84	35
Region 3	6.50	7.02	11	7.20	5

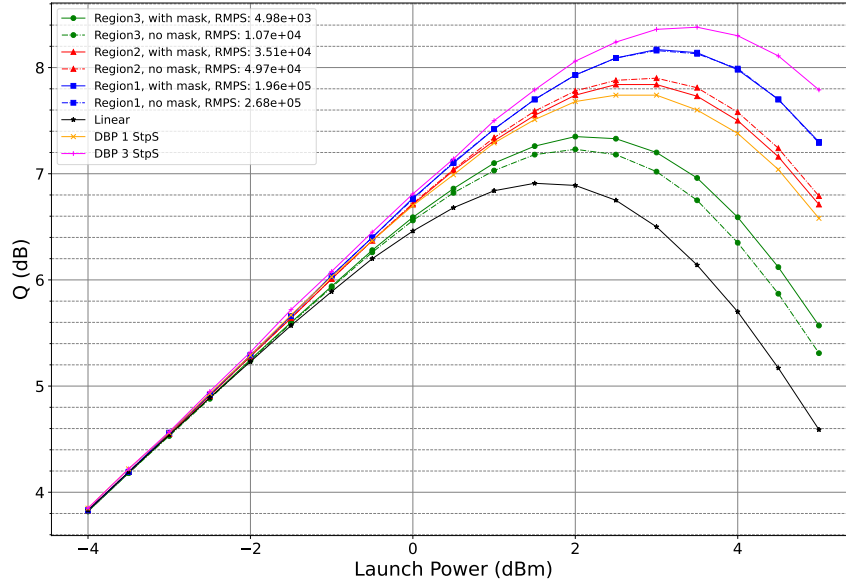


Fig. 10. Performance of selected 64QAM models for the three different regions of Table 5 at various launch powers . The results of the linear compensation and DBP with 1 and 3 steps per span are also shown in the figure.

5. Conclusion

In this work, by using Transformers, we introduced a new nonlinear channel equalization method based on the self-attention mechanism. We showed that in order to leverage parallel computation and attending directly to the memory across a sequence of symbols, Transformers can be used effectively for coherent long-haul transmissions. Efficient embedding and detailed implementation of Transformers as well as the use of a physics-informed mask were presented. Moreover, the designs were optimized for block-processing in order to meet the practical high-throughput low-latency requirements of optical transmission. The designs were supported with numerical results which show that one can use the Transformer-NLCs as an efficient, flexible and parallel method to compensate the channel nonlinearity. The next step is simplifying the Transformer-NLC design. One possible approach is to modify the attention structure by deigning more efficient kernel-based formulation of the self-attention. Furthermore, the impacts of quantization and pruning need to be studied for the real-world processing through both post-training simplification and quantization-aware training. This includes the impact on masked Transformers as well since the importance in perturbation coefficients are centralized for each position so even with mask, we would have smaller values in the attention matrix.

References

1. E. Ip and J. M. Kahn, "Compensation of dispersion and nonlinear impairments using digital backpropagation," *J. Light. Technol.* **26**, 3416–3425 (2008).
2. L. B. Du and A. J. Lowery, "Improved single channel backpropagation for intra-channel fiber nonlinearity compensation in long-haul optical communication systems," *Opt. Express* **18**, 17075–17088 (2010).
3. E. F. Mateo, F. Yaman, and G. Li, "Efficient compensation of inter-channel nonlinear effects via digital backward propagation in WDM optical transmission," *Opt. Express* **18**, 15144–15154 (2010).
4. A. Mecozzi and R.-J. Essiambre, "Nonlinear Shannon limit in pseudolinear coherent systems," *J. Light. Technol.* **30**, 2011–2024 (2012).
5. Z. Tao, L. Dou, W. Yan, L. Li, T. Hoshida, and J. C. Rasmussen, "Multiplier-free intrachannel nonlinearity compensating algorithm operating at symbol rate," *J. Light. Technol.* **29**, 2570–2576 (2011).
6. S. Zhang, F. Yaman, K. Nakamura, T. Inoue, V. Kamalov, L. Jovanovski, V. Vusirikala, E. Mateo, Y. Inada, and T. Wang, "Field and lab experimental demonstration of nonlinear impairment compensation using neural networks," *Nat. Commun.* **10**, 1–8 (2019).
7. C. Häger and H. D. Pfister, "Nonlinear interference mitigation via deep neural networks," in *Optical fiber communication conference*, (Optical Society of America, 2018), pp. W3A–4.
8. O. Sidelnikov, A. Redyuk, S. Sygletos, M. Fedoruk, and S. Turitsyn, "Advanced convolutional neural networks for nonlinearity mitigation in long-haul WDM transmission systems," *J. Light. Technol.* **39**, 2397–2406 (2021).
9. S. Deligiannidis, A. Bogris, C. Mesaritis, and Y. Kopsinis, "Compensation of fiber nonlinearities in digital coherent systems leveraging long short-term memory neural networks," *J. Light. Technol.* **38**, 5991–5999 (2020).
10. P. J. Freire, Y. Osadchuk, B. Spinnler, A. Napoli, W. Schairer, N. Costa, J. E. Prilepsky, and S. K. Turitsyn, "Performance versus complexity study of neural network equalizers in coherent optical systems," *J. Light. Technol.* **39**, 6085–6096 (2021).
11. A. Bakhshali, H. Najafi, B. B. Hamgini, and Z. Zhang, "Neural network architectures for optical channel nonlinear compensation in digital subcarrier multiplexing systems," *arXiv preprint arXiv:2304.06836* (2023).
12. H. Ming, X. Chen, X. Fang, L. Zhang, C. Li, and F. Zhang, "Ultralow complexity long short-term memory network for fiber nonlinearity mitigation in coherent optical communication systems," *J. Light. Technol.* **40**, 2427–2434 (2022).
13. P. J. Freire, A. Napoli, D. A. Ron, B. Spinnler, M. Anderson, W. Schairer, T. Bex, N. Costa, S. K. Turitsyn, and J. E. Prilepsky, "Reducing computational complexity of neural networks in optical channel equalization: From concepts to implementation," *J. Light. Technol.* (2023).
14. A. Vaswani, N. Shazeer, N. Parmar, J. Uszkoreit, L. Jones, A. N. Gomez, L. Kaiser, and I. Polosukhin, "Attention is all you need," *Adv. Neural Inf. Process. Syst.* **30** (2017).
15. P. K. A. Wai and C. Menyak, "Polarization mode dispersion, decorrelation, and diffusion in optical fibers with randomly varying birefringence," *J. Light. Technol.* **14**, 148–157 (1996).
16. Y. Gao, J. C. Cartledge, A. S. Karar, S. S.-H. Yam, M. O'Sullivan, C. Laperle, A. Borowiec, and K. Roberts, "Reducing the complexity of perturbation based nonlinearity pre-compensation using symmetric EDC and pulse shaping," *Opt. Express* **22**, 1209–1219 (2014).
17. I. Hubara, M. Courbariaux, D. Soudry, R. El-Yaniv, and Y. Bengio, "Quantized neural networks: Training neural networks with low precision weights and activations," *The J. Mach. Learn. Res.* **18**, 6869–6898 (2017).
18. P. J. Freire, D. Abode, J. E. Prilepsky, N. Costa, B. Spinnler, A. Napoli, and S. K. Turitsyn, "Transfer learning for neural networks-based equalizers in coherent optical systems," *J. Light. Technol.* **39**, 6733–6745 (2021).
19. D. Bahdanau, K. Cho, and Y. Bengio, "Neural machine translation by jointly learning to align and translate," *arXiv preprint arXiv:1409.0473* (2014).
20. A. Katharopoulos, A. Vyas, N. Pappas, and F. Fleuret, "Transformers are RNNs: Fast autoregressive Transformers with linear attention," in *International Conference on Machine Learning*, (PMLR, 2020), pp. 5156–5165.
21. S. Zhai, W. Talbott, N. Srivastava, C. Huang, H. Goh, R. Zhang, and J. Susskind, "An attention free transformer," *arXiv preprint arXiv:2105.14103* (2021).
22. R. Xiong, Y. Yang, D. He, K. Zheng, S. Zheng, C. Xing, H. Zhang, Y. Lan, L. Wang, and T. Liu, "On layer normalization in the Transformer architecture," in *International Conference on Machine Learning*, (PMLR, 2020), pp. 10524–10533.
23. R. Child, S. Gray, A. Radford, and I. Sutskever, "Generating long sequences with sparse transformers," *arXiv preprint arXiv:1904.10509* (2019).
24. I. Beltagy, M. E. Peters, and A. Cohan, "Longformer: The long-document transformer," *arXiv preprint arXiv:2004.05150* (2020).
25. G. P. Agrawal, "Nonlinear fiber optics," 2nd ed., New York: Acad. (1995).

A. Impact of Model’s Hyper-Parameters

We present a deeper study on the impacts of different hyper-parameters on the performance of Transformer-NLC in this appendix. For brevity, we limit out the scope of result presentation here to the 16QAM setup at 2 dBm launch power.

A.1. Embedding Type

As mentioned in Section 3.2, we have explored two types of embedding-generator module, one with MLPs and one with CNNs. Two configurations were used for the MLP: one MLP has only a linear layer which maps the input symbols ($R^{(2t+b) \times 4}$) to the embeddings ($R^{(\ell+b) \times d_{model}}$). The other one has two linear layers where the first one maps the input symbols ($R^{(2t+b) \times 4}$) to intermediate representations ($R^{(\ell+b) \times d_{interm}}$) and the second layer maps those to embeddings ($R^{(\ell+b) \times d_{model}}$). There is also an activation function (Leaky ReLU) between the two linear layers for the second MLP configuration. Note that over the input symbol sequence, the MLPs are applied to each position, similarly. Furthermore, to employ the feature extraction capability of CNNs, a CNN configuration is tested for generating embeddings where we use one convolutional layer with four input channel and d_{model} output channels, a kernel size of nine and a stride of one. A Leaky ReLU activation is used after the convolutional layer.

Table 6 shows the impact of three different embedding-generator module types on Q and RMPS. These results were obtained by a Transformer with the block size of 128, tap, key, hidden, and FFN hidden sizes of 64, and a window size of 7 for window processing. As it can be seen from the table, the CNN embedding generator module has a large positive impact on the model prediction capability with close RMPS value to the two MLP embedding generator modules.

Another interesting observation comes from the implications of using mask. When a mask was used, the performance of the model with CNN generated embeddings did not decrease significantly in contrast to the MLP generated embeddings. Similar trend was observed for other performance and complexity regions. Therefore, throughout the paper, CNN embedding generator module were selected as the default choice in order to simplify the presentation.

Table 6. Impact of the embedding type on performance for a Transformer with block size of 128, tap, key, hidden and FFN hidden sizes of 64, and a window size of 7.

Embedding	Q	No Mask		Mask with $\rho = 2.6$	
		Q _{NN}	RMPS (K)	Q _{NN}	RMPS (K)
1 Layer MLP	6.67	8.01	368	7.34	241
2 Layer MLP	6.67	8.17	372	7.23	245
CNN	6.67	8.72	354	8.70	222

A.2. Block Size

As we discussed in Eq. (5), the computational complexity of a Transformer changes with the input block size. To investigate its impact, we trained models with block sizes $b \in \{16, 32, 64, 128\}$ in this part. Fig. 11 shows the envelope of evaluated performance over different RMPS regions for the various block sizes. It can be seen here that as the block size increases, the performance envelopes shift to the lower complexity regions. We also do not observe a decrease or cap on the best performances. This indicates that the block training approach is resilient and does not suffer by increasing the block size. Furthermore, it is apparent that the use of a mask is beneficial for all block sizes at almost all complexity regions except at the tail of high complexity region where extra symbols can provide minimal advantages specially at smaller block sizes.

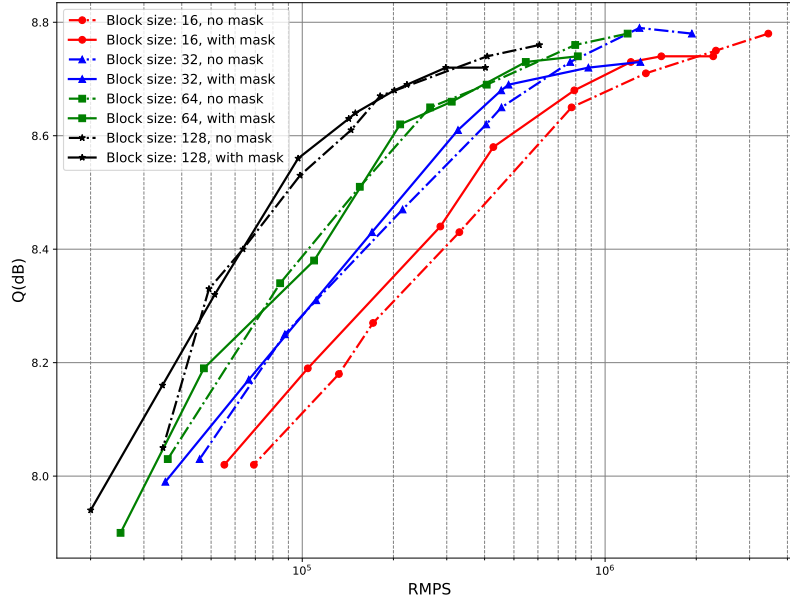


Fig. 11. Impact of block size on the Transformer-NLCs.

For comparison, with an example we show the performance and complexity of Transformers with and without masks for the selected block sizes in Table 7. Note that the rest of the hyper-parameters are fixed in this case.

Table 7. Impact of block size on the Transformer-NLCs. Other hyper-parameters are as following: FFN hidden size = 64, hidden size = 64, key size = 64, window size = 15, number of heads = 4, tap size = 96.

block size	Q	No Mask		Mask with $\rho = 2.6$	
		Q_{NN}	RMPS (K)	Q_{NN}	RMPS (K)
16	6.67	8.70	2039	8.73	1216
32	6.67	8.77	1141	8.70	711
64	6.67	8.71	708	8.69	451
128	6.67	8.71	511	8.68	307

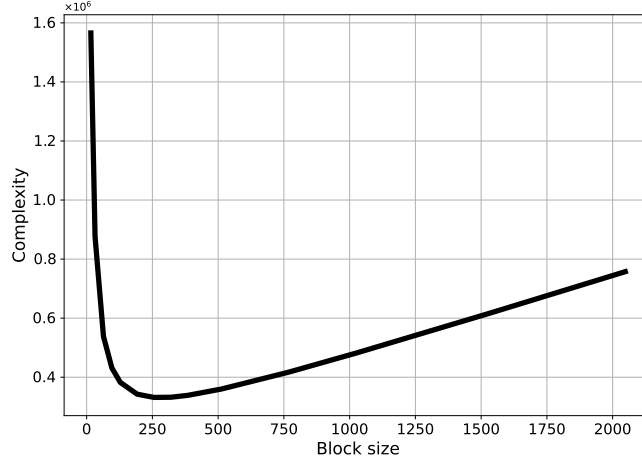


Fig. 12. Complexity versus block size for a Transformer where all the hyper-parameters are fixed except the block size. Tap size = 96, hidden size = 64, key size = 64, FFN hidden size = 64, number of heads = 4, and number of encoder layers = 2.

By investigating Eq. (5), we may expect that the complexity of a Transformer increases as we increase the block size. However, the graph and table show something different. To understand this, we analyze Eq. (5) for the cases where all the hyper-parameters are constant except the block size. We can rewrite this equation as follows:

$$RMPS_{att-blk} = \frac{c_1(\ell + b)^2}{b} \quad (8)$$

where $c_1 = hd_k + 3h$ and $N = \ell + b$. By expanding the above equation and after canceling out the common terms, we obtain

$$RMPS_{att-blk} = 2c_1\ell + \frac{c_1\ell^2}{b} + c_1b \quad (9)$$

where the first term is independent of the block size, the second term decreases as the block size increases (rectangular hyperbola) while the third term linearly increases as the block size increases. Therefore, at smaller block sizes, the second term decreases more rapidly compared to the third term which is linear. However, at larger block sizes, the linear part (third term) grows larger than the rectangular hyperbola (second term) and as the block sizes increase, the overall complexity increases.

For illustration purpose, Fig. 12 shows the complexity of a Transformer with respect to the block size, while all the other hyper-parameters are constant. The figure corroborates our claims by showing that as the block size is increased, the complexity reduces to a global minimum after which the linear term dominates and we see an increase in the complexity as the block size is increased further. It should also be noted that there are other types of Transformers where their attention computation's complexity is of order of $O(Nd_{model})$ [20, 21]. In those Transformers, the complexity should be reduced by increasing the block size.

A.3. Hidden Size

The hidden size (the size of embeddings or d_{model}) impacts the Transformer's accuracy and computational complexity. A small hidden size may not be able to capture the memory of nonlinear channel, although it decreases the computational complexity. On the other hand, a very large hidden size will inflate the complexity while may not necessarily increase the performance. Figure 13 shows the effect of hidden size on the performance versus complexity. As it can be seen from this figure, at the lower complexities, there is a loss on the envelope of performance when the mask is not used to optimize the complexity for the limited available resources. However, at the higher complexity regions, the required hidden size is saturated and there is no gap related to use of mask on the envelope of performance. For the selected setup, to maximize the performance, hidden size of 64 is the best option overall which covers a wide range of complexity while giving the best performance.

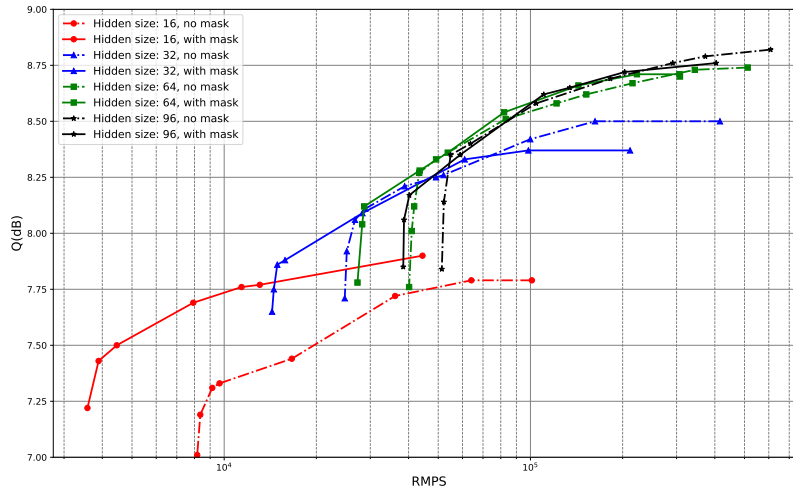


Fig. 13. Impact of the hidden size on the Transformer-NLCs.

A.4. Tap Size

As we discussed in Section 3, we need to provide the surrounding input symbols to the model in order to compute the nonlinear interference in form of E_{XI} and E_{XQ} for a target symbol at the output of Transformer. This is mainly due to the channel memory from the accumulated dispersion during fiber propagation. The number of these surrounding symbols are determined by the tap size. We trained models with various tap sizes where the results are depicted in Fig. 14. As it can be seen here, for higher complexities, the tap sizes of 64 and 96 provide better performances while among them, the tap size of 64 covers a wider range of complexities. Furthermore, with a large enough tap size, the use of a mask has almost no impact at the higher performances while provides complexity advantage on the lower side of the performance envelope.

Note that for each taps size, the performance envelopes for Transformers with and without mask demonstrate a crossing complexity threshold. Below that threshold, the use of a mask provides superior performance while for models with higher complexity the use of mask demonstrates some performance loss especially at lower tap sizes. This loss can be attributed to the extended interactions across neighboring symbols through the block-processing structure where the symbols in the middle of the block still have connections to a larger than defined tap size inside attention calculation. However, this extended tap size is blocked with the use of a mask. Therefore, for a

given small tap size at higher complexity region, it is better to avoid using a mask to be able to access information from more neighboring symbols in the block-processing approach.

Generally at lower complexity regions, one should reduce the tap size in order to achieve better performances as seen by performance curves associated to 16 and 32 tap sizes. Also note that on the overall envelope of performance versus complexity with union over all tap sizes, for each complexity value, one can still get a better performance with a masked structure if a large enough tap size is selected. In other words, the best performance curve across all tap sizes is defined by the masked models.

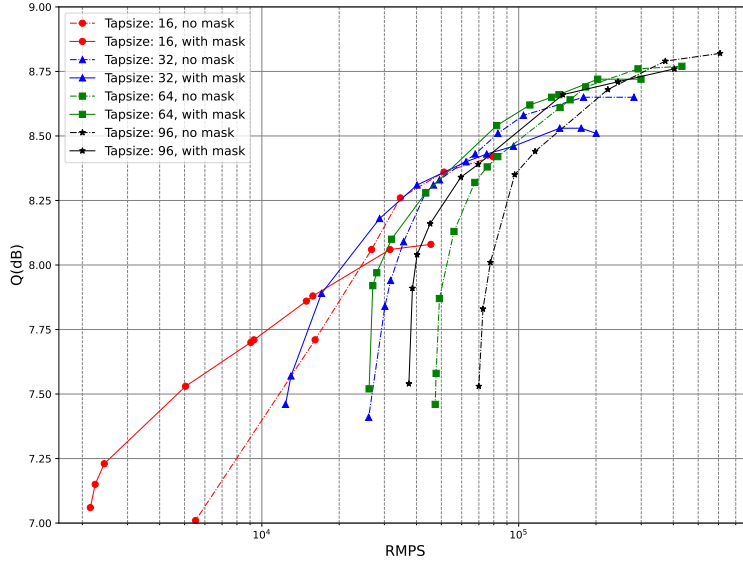


Fig. 14. Impact of the tap size on the Transformer-NLCs.

A.5. Number of Layers

As discussed in Section 2.2 and depicted in Fig. 2, the core of Transformers can be stacked in several layers which linearly scales the computational complexity provided that the other parameters are unchanged. In order to see the impact of number of layers in the Transformer-NLCs on the performance, we ran simulations on transformers with one to three layers and explored the performance-complexity trade-off for each design. The results for the 16QAM setup case are depicted in Fig. 15. One can conclude from this figure that Transformers with three layers of encoder perform slightly better compared to the ones with two layers of encoder at high complexity regions. However, for a wide range of complexities, the two-layer configuration is the best model to achieve the performance envelope. Moreover, the use of a mask generally improves the performance at the lower complexity regions and extends the savings in resources as we move to the lower complexity limits.

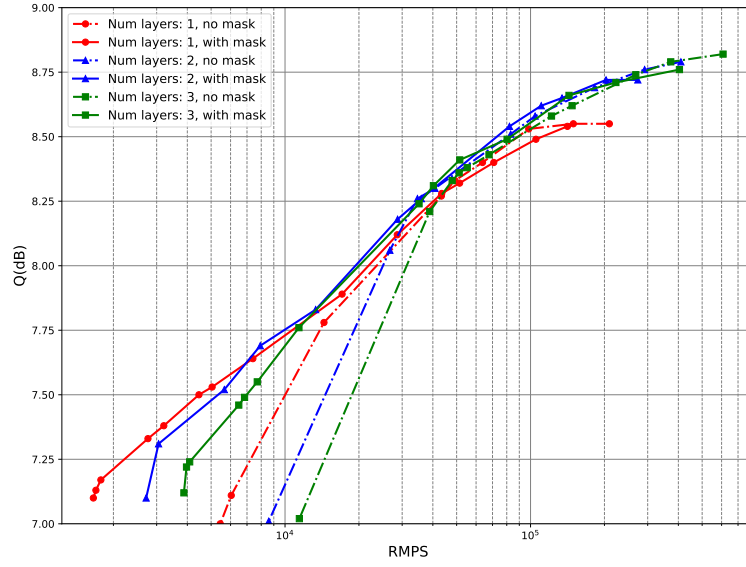


Fig. 15. Impact of the number of encoder layers on the Transformer-NLCs.

A.6. Number of Heads

The impact of number of heads in the multi-head attention structure is studied next. We have tested one, two, and four heads to see their impacts on the performance versus complexity trade-off curves. In general, a higher number of heads increases the parallelization capabilities of the Transformer while slightly improves the performance. Results for the selected cases are depicted in Fig. 16. This figure shows that for a wide range of complexities, a higher number of attention heads results in slightly better performance for the same complexity. Also as observed before, the use of a mask has no significant impact on the overall conclusion while it can improve the performance at lower complexity regions.

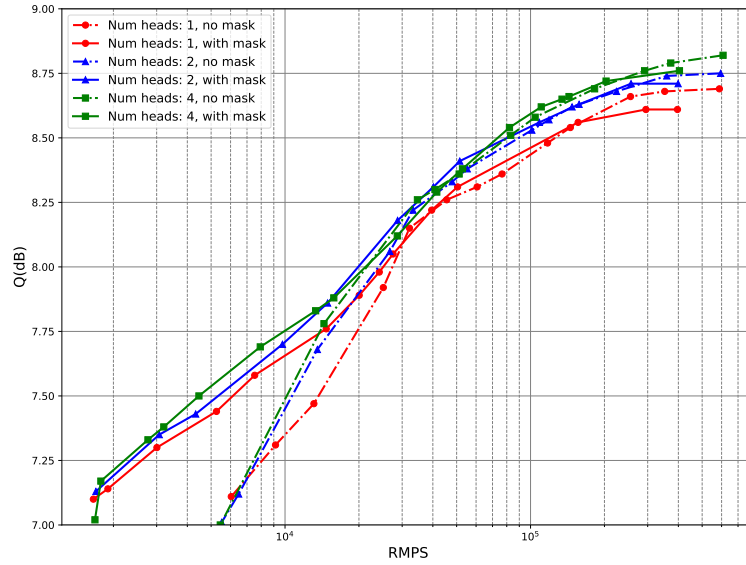


Fig. 16. Impact of the number of heads on the Transformer-NLCs.

A.7. Number of Neighbors at the Output Layer

Finally, we explore the impact of varying the number of neighbors, $2w$, or equivalently changing the window size $W = 2w + 1$ on the performance and complexity of Transformers as explained in a Section 3.4. The results are depicted in Fig. 17. As the figure shows, increasing the window size can provide a gain in performance of up to 0.2 dB over a wide range of complexities. Note that a window size of 7 seems to be optimal for mid and high complexity regions. It can also be noted that increasing the window size is not beneficial especially at lower complexity regions where the extra information on the last layer is not helpful if the core of Transformer is limited in resources. Also, the use of a mask follows the general conclusion that a mask can improve the performance at lower complexities.

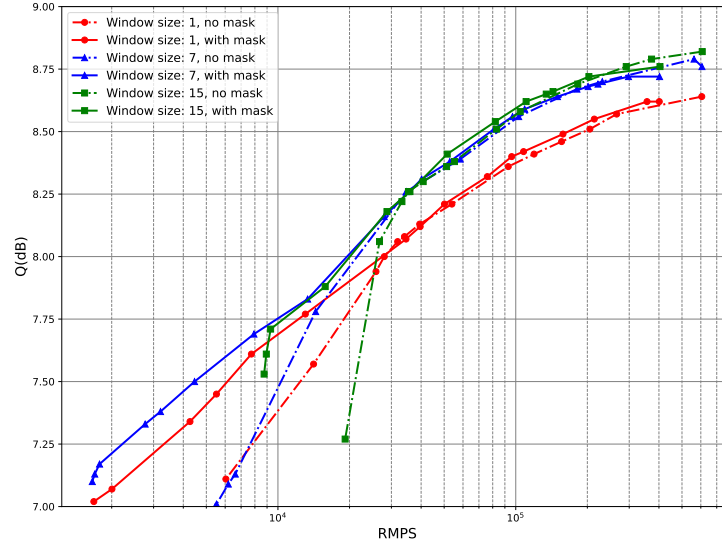


Fig. 17. Impact of the window size at the output layer on the Transformer-NLCs.

B. Attention Heat Maps

In this appendix, we show several two-dimensional heat maps of $(QK^T)/\sqrt{d_k}$ (scaled multiplication of the queries and keys) with and without mask prior to the application of softmax function. Fig 18 illustrates $(QK^T)/\sqrt{d_k}$ values averaged over a batch for a Transformer with three encoder layers and four heads. As seen in this figure, the majority of large values of $(QK^T)/\sqrt{d_k}$ is around the main diagonal, which confirms that one can reduce the computational complexity by using the proposed masks. Thus, by using block masks we force some elements of attention matrix to zero which can reduce the computational complexity considerably. Fig. 19 shows the $(QK^T)/\sqrt{d_k}$ values averaged over a batch for $\rho = 2.6$. Furthermore, Fig. 20 shows another example of heat maps for a Transformer with three encoder layers and a single head.

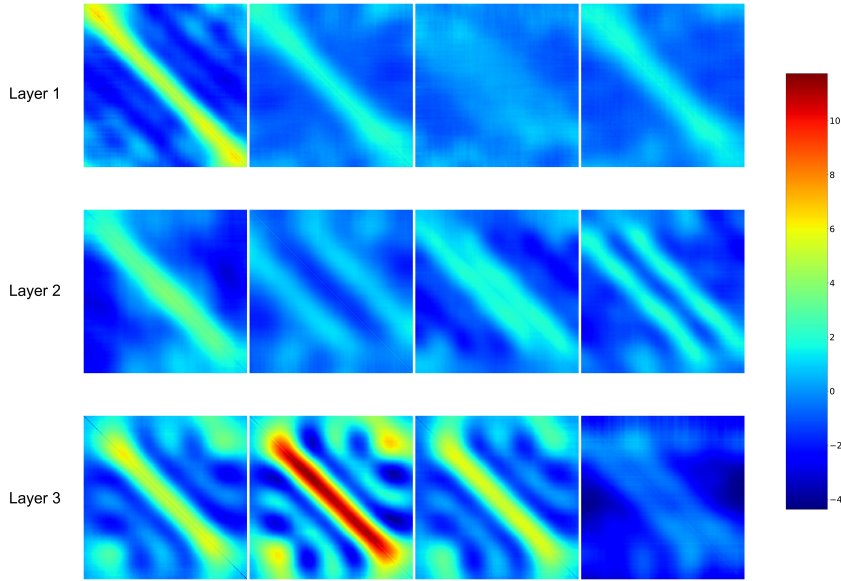


Fig. 18. The 2D matrix $(QK^T)/\sqrt{d_k}$ averaged over a batch for a Transformer with 3 encoder layers and 4 heads. Rows show the values for 3 layers and columns show the values for 4 heads. The spectrum from red to blue represents high to low values.

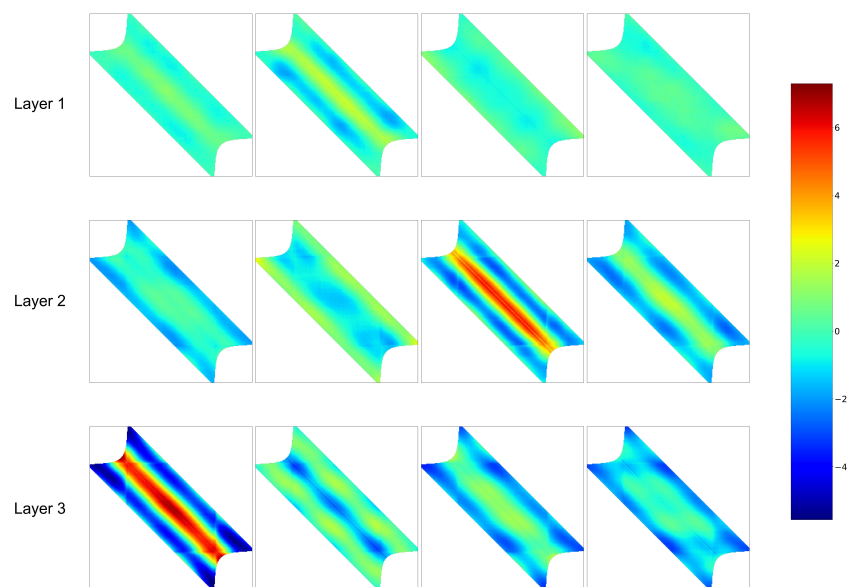


Fig. 19. The 2D matrix $(QK^T)/\sqrt{d_k}$ averaged over a batch with mask for a Transformer with 3 encoder layers and 4 heads. Rows show the values for 3 layers and columns show the values for 4 heads. In this figure ρ is equal to 2.6. White area shows elements with negative infinity values.

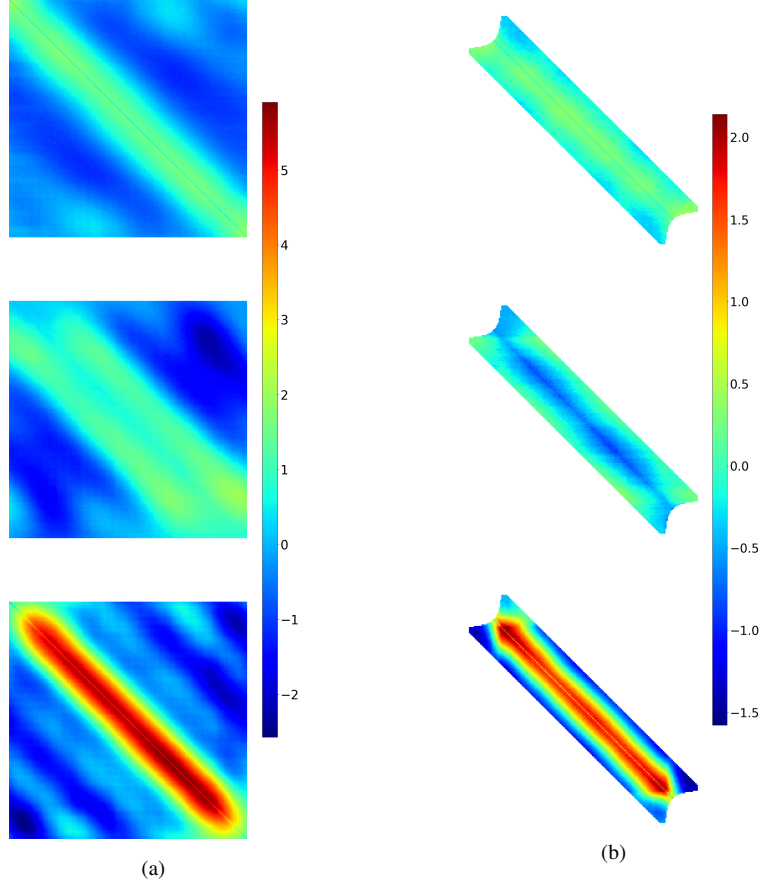


Fig. 20. Heat maps for the attention matrices. The 2D matrix $(QK^T)/\sqrt{d_k}$ averaged over a batch for a Transformer with 3 encoder layers and 1 head. Rows show the values for 3 layers. The spectrum from red to blue represents high to low values. (a) shows the attention matrix for a Transformer without any masks and (b) is the attention matrix for a Transformer with the same hyper-parameters as (a) but with the proposed mask with ρ equal to 2.6.